Nonlin. Processes Geophys. Discuss., https://doi.org/10.5194/npg-2017-48
Manuscript under review for journal Nonlin. Processes Geophys.
Discussion started: 26 September 2017

Nonlinear Processes in Geophysics
Discussions
Open Access
EGU

Tipping point analysis of ocean acoustic noise

Valerie N. Livina[1], Albert Brouwer[2], Peter Harris[1], Lian Wang[1], Kostas Sotirakopoulos[1], and Stephen Robinson[1]

[1]National Physical Laboratory, Teddington, Middlesex TW11 0LW, UK
[2]Preparatory Commission of the Comprehensive Nuclear-Test-Ban Treaty Organization, Vienna, Austria

Correspondence to: Valerie Livina
(valerie.livina@npl.co.uk)

Abstract. We apply tipping point analysis to a large record of ocean acoustic data to identify the main components of the acoustic dynamical system and study possible bifurcations and transitions of the system. The analysis is based on a statistical physics framework with stochastic modelling, where we represent the observed data as a composition of deterministic and stochastic components estimated from the data using time series techniques. We analyse long-term and seasonal trends, system states and acoustic fluctuations to reconstruct a one-dimensional stochastic equation to approximate the acoustic dynamical system. We apply potential analysis to acoustic fluctuations and detect several changes in the system states in the past 14 years. These are most likely caused by climatic phenomena. We analyse trends in sound pressure level within different frequency bands and hypothesise a possible anthropogenic impact on the acoustic environment. The tipping point analysis framework provides insight into the structure of the acoustic data and helps identify its dynamic phenomena, correctly reproducing the probability distribution and scaling properties (power-law correlations) of the time series.

Keywords. time series analysis — tipping point analysis — stochastic modelling — acoustic data — El Niño

1 Introduction

The Preparatory Commission of the Comprehensive Nuclear-Test-Ban Treaty Organization (CTBTO) has established a global network of underwater hydrophones as a part of its hydroacoustic observations (others being seismic, infrasound, and radionuclide), with the goal of continuous monitoring for possible nuclear explosions (CTBTO 2013). The CTBTO database provides several unique and

Nonlin. Processes Geophys. Discuss., https://doi.org/10.5194/npg-2017-48
Manuscript under review for journal Nonlin. Processes Geophys.
Discussion started: 26 September 2017

large oceanic acoustic records, covering more than ten years of continuous recording with a high temporal resolution of 250 Hz. In this article, we study the records of the hydrophone H01W1 at the Cape Leeuwin station. The hydrophone is located at a depth of about 1 km off the south-west shore of Australia. We apply tipping point analysis and identify the main components of this acoustic dynamical system, which we then model, with reconstruction of the probability distribution and scaling properties (power-law correlations) of the observed data. Both the probability distribution and scaling properties are important for ensuring that the model correctly represents the observed data, because probability distribution characterises the range and frequency of time series values, while scaling properties characterise their temporal arrangement (Kantelhardt et al 2002), (Livina et al 2013).

Tipping points in climatic subsystems have become a widely publicised topic of high societal interest related to climate change; see, for example, (Lenton et al 2008). Applications of tipping point analysis have been found in geophysics (Livina and Lenton 2007), (Lenton et al 2009), (Livina et al 2010), (Livina et al 2011), (Livina et al 2012), (Lenton et al 2012a), (Lenton et al 2012b), (Livina et al 2013), (Cimatoribus et al 2013), (Livina et al 2013), statistical physics (Vaz Martins et al 2010), (Livina et al 2013), ecology (Dakos et al 2012), and structure health monitoring (Livina et al 2014), (Perry et al 2016).

A stochastic model combining deterministic and stochastic components is a powerful yet simple tool for modelling time series of real-world dynamical systems. Given a one-dimensional trajectory of a dynamical system (the recorded time series), the system dynamics can be modelled by the stochastic equation with state variable z and time t:

$$\dot{z} = D(z,t) + S(z,t), \tag{1}$$

where $\dot{z}$ is the time derivative of the system variable $z(t)$, and D and S are deterministic and stochastic components, respectively. Component $D(z,t)$ may be stationary or dynamically changing (for instance, containing long-term and/or periodic trends). Many geophysical variables, which follow seasonal variability, can be approximated by a stochastic model

$$z(t) = T(t) + A(t)\cos(2\pi\phi(t)) + \Phi(t), \tag{2}$$

where the trend $T(t)$ is a real-valued function, such as a straight-line function of t, the second term models seasonal variability, and $\Phi(t)$ is a stationary random process. As an example, $\Phi(t)$ can be Gaussian white noise or a continuous autoregressive moving average random process of order (p,q). Similarly, (De Livera et al 2011) used a trigonometric Box-Cox transform with ARMA errors and seasonal components.

The probability distribution of the trajectory (time series) of such a system, however complex it may be, can in the majority of cases be approximated using a so-called system potential in the form of a polynomial of even order. Tipping points can be identified in terms of the variability of the underlying system potential $U(z,t)$, which defines (if it exists) the deterministic term in Equation

Nonlin. Processes Geophys. Discuss., https://doi.org/10.5194/npg-2017-48
Manuscript under review for journal Nonlin. Processes Geophys.
Discussion started: 26 September 2017

Nonlinear Processes in Geophysics
Discussions
Open Access
EGU

(1): $D(z,t) = -U'(z,t)$. If the structure of the potential (the number of potential wells) changes, the tipping point is a bifurcation. If the potential structure remains the same, while the trajectory of the system samples various states, such a tipping point is transitional (Livina et al 2011). The stochastic component, in the simplest case, may be Gaussian white or red noise, with possible multifractality and other nonlinear properties. The tipping point methodology is currently based on the techniques of degenerate fingerprinting and potential analysis, which are described below.

2 Methodology

The tipping point analysis consists of the following three stages: 1) anticipating (pre-tipping, or analysis of early warning signals), 2) detecting (tipping), and 3) forecasting (post-tipping).

Anticipating tipping points (pre-tipping) is based on the effect of slowing down of the dynamics of the system prior to critical behaviour. When a system state becomes unstable and starts a transition to another state, the response to small perturbations becomes slower. This critical slowing down can be detected as increasing autocorrelations (ACF) in the time series (Held and Kleinen 2004). Alternatively, the short-range scaling exponent of Detrended Fluctuation Analysis (DFA) (Peng et al 1994) may be monitored (up to 100 units, which in the case, for example, of daily data correspond to 3.5 months, see (Livina and Lenton 2007)). The lag-1 autocorrelation is calculated in sliding windows of fixed length (conventionally, half of the series length) or variable length (for uncertainty estimation) along the time series, which produces a curve of an early warning indicator. This indicator describes the structural dynamics of the time series. If the curve of the indicator remains flat and stable, the time series does not experience a critical change (whether bifurcational or transitional). If the indicator rises to a critical value of 1 (the monotonic trend can be estimated, for instance, using Kendall rank correlation), it provides a warning of critical behaviour.

Lag-1 autocorrelation is estimated by fitting an autoregressive process of order 1 (AR1):

$$z_{t+1} = cz_t + \sigma\eta_t \tag{3}$$

where η is a Gaussian white noise process of unit variance, σ is the noise level, and $c = e^{-\kappa\Delta t}$ is the ACF-indicator with κ the decay rate of perturbations. Then, $c \to 1$ as $\kappa \to 0$ when a tipping point is approached. In addition, the DFA method utilises built-in detrending of a chosen polynomial order, which allows one to distinguish transitions and bifurcations in the early-warning signals. This can be done by comparing several early-warning indicators, with and without detrending data in sliding windows (Livina et al 2012). The paper (Livina and Lenton 2007) provided the first application of the DFA-based early warning indicator to the paleotemperature record with detected transition using both ACF and DFA indicators.

Detecting and **forecasting** of a tipping point is performed using dynamical potential analysis. The technique detects a bifurcation in a time series and the time when it happens, which is illustrated in a novel plot mapping by colour the potential dynamics of the system (Livina et al 2010), (Livina

Nonlin. Processes Geophys. Discuss., https://doi.org/10.5194/npg-2017-48
Manuscript under review for journal Nonlin. Processes Geophys.
Discussion started: 26 September 2017

et al 2011). The dynamics of the tipping point is forecast using extrapolation of the dynamically derived Chebyshev coefficients of the approximation to the probability density function of the system trajectory (Livina et al 2013).

For the purposes of potential analysis, the dynamics of the system is approximated by a potential stochastic model with a polynomial U (which, in general, may depend on both state variable z and time):

$$\dot{z} = -U'(z,t) + \sigma\eta, \tag{4}$$

where $\dot{z}$ is the time derivative of the system variable $z(t)$, η is Gaussian white noise of unit variance and η is the noise level. In the case of a double-well potential, U can be described by a polynomial of 4th order (assuming its quasi-stationarity, with dependence on the state variable z only):

$$U(z) = a_4 z^4 + a_3 z^3 + a_2 z^2 + a_1 z, \tag{5}$$

The Fokker-Planck equation for the probability density function $p(z,t)$,

$$\delta_t p(z,t) = \delta_z [U'(z) p(z,t)] + \frac{1}{2}\sigma^2 \delta_z^2 p(z,t), \tag{6}$$

has a stationary solution given by

$$p(z,t) \sim \exp\left[-2U(z)/\sigma^2\right]. \tag{7}$$

The potential can be reconstructed from time series data of the system using the following relation to the probability density function:

$$U(z) = -\frac{\sigma^2}{2} \log p_d(z), \tag{8}$$

which means that the empirical probability density p_d (kernel distribution) has a number of modes corresponding to the number of wells of the potential.

The structural changes of the potential are often not visible in the time series, yet they may lead to a dramatic evolution of the system. Detecting such changes gives an advantage in understanding of the dynamical system. The potential coloured map (Livina et al 2010) visualises bifurcations according to the number of detected system states. It illustrates bifurcations as the change in the colour describing the number of states along all time-scales (the y-axis shows the length of the sliding window of data for which the number of states is assessed). If no such pattern is observed, there is no bifurcation in the time series.

This stochastic approximation of the system structural dynamics has remarkable accuracy for data subsets of length as short as 400 to 500 data points, demonstrating above 90% rate of successful detection, as was shown in an experiment with double-well-potential artificial data (Livina et al 2011). For data subsets of length greater than 1000 data points it correctly detects the structure of the potential with a success rate of over 98%.

Nonlin. Processes Geophys. Discuss., https://doi.org/10.5194/npg-2017-48
Manuscript under review for journal Nonlin. Processes Geophys.
Discussion started: 26 September 2017

The technique of potential forecasting is based on dynamical propagation of the probability density function of the time series. We employ the coefficients of the Chebyshev polynomial approximation of the empirical probability distribution and extrapolate them in order to forecast the future probability distribution of the data. After reconstruction of the system kernel distribution, a time series is generated using rejection sampling technique, and then the obtained dataset is sorted according to the initial data in order to reconstruct the temporal correlations in the time series. The detailed mathematical description of the potential forecasting technique is given in (Livina et al 2013). The technique has the advantage of reproducing both static properties (probability density) and dynamic properties (scaling exponent, or power-law correlations) of a time series.

3 Data

We study the large CTBTO record (2003-2016) of the Cape Leeuwin hydrophone, series H01W1, which is a 250 Hz-sampled time series of ocean sound pressure. The raw data represents 3 Tb of binary waveforms, which after extraction constitute 95 billion points in the time series. We analyse 1-minute averages of sound pressure level (SPL) in five frequency bands (broadband, 10-30 Hz, 40-60 Hz, 56-70 Hz, and 85-105 Hz), of about 7 million points per time series. This data has pronounced seasonality and some small gaps, and therefore we perform interpolation and deseasonalisation of all five time series, the result of which can be seen in Figure 1.

The data samples were scaled using their calibration factors (provided by CTBTO), and an inverse filter of the recording systems frequency response was applied to eliminate the effect of the acquisition chain on the frequency response of the recordings. The Fast Fourier Transform of the signal was computed using rectangular windows of 15 thousand samples (i.e. 1-minute-long intervals at 250 Hz sampling rate) and the broadband signal was then filtered in 5 frequency bands (5-115 Hz, 10-30 Hz, 40-60 Hz, 56-70 Hz, 85-105 Hz) via selection of the corresponding FFT bins within each frequency band. Then the resulting Sound Pressure Level (SPL) in dB re 1 μ Pa^2 for each frequency band was calculated (Robinson et al 2014), (ISO 18405:2017). Finally, outliers, i.e. levels greater than 20 dB from the average of the entire time series of SPL values, were removed.

Because of the data gaps, we interpolate the SPL data to achieve equidistant 1-minute temporal resolution. We then remove the seasonal periodicity by subtracting the averaged seasonal cycle over the 14 years of observation to obtain the fluctuations

$$z_i = S_i - \bar{S}_i, \tag{9}$$

where S_i is the interpolated SPL data, and $\bar{S}_i$ is the mean 1-minute interpolated SPL data. The resulting fluctuations are shown in the right column of Figure 1, for the broadband and four selected sub-bands.

Nonlin. Processes Geophys. Discuss., https://doi.org/10.5194/npg-2017-48
Manuscript under review for journal Nonlin. Processes Geophys.
Discussion started: 26 September 2017

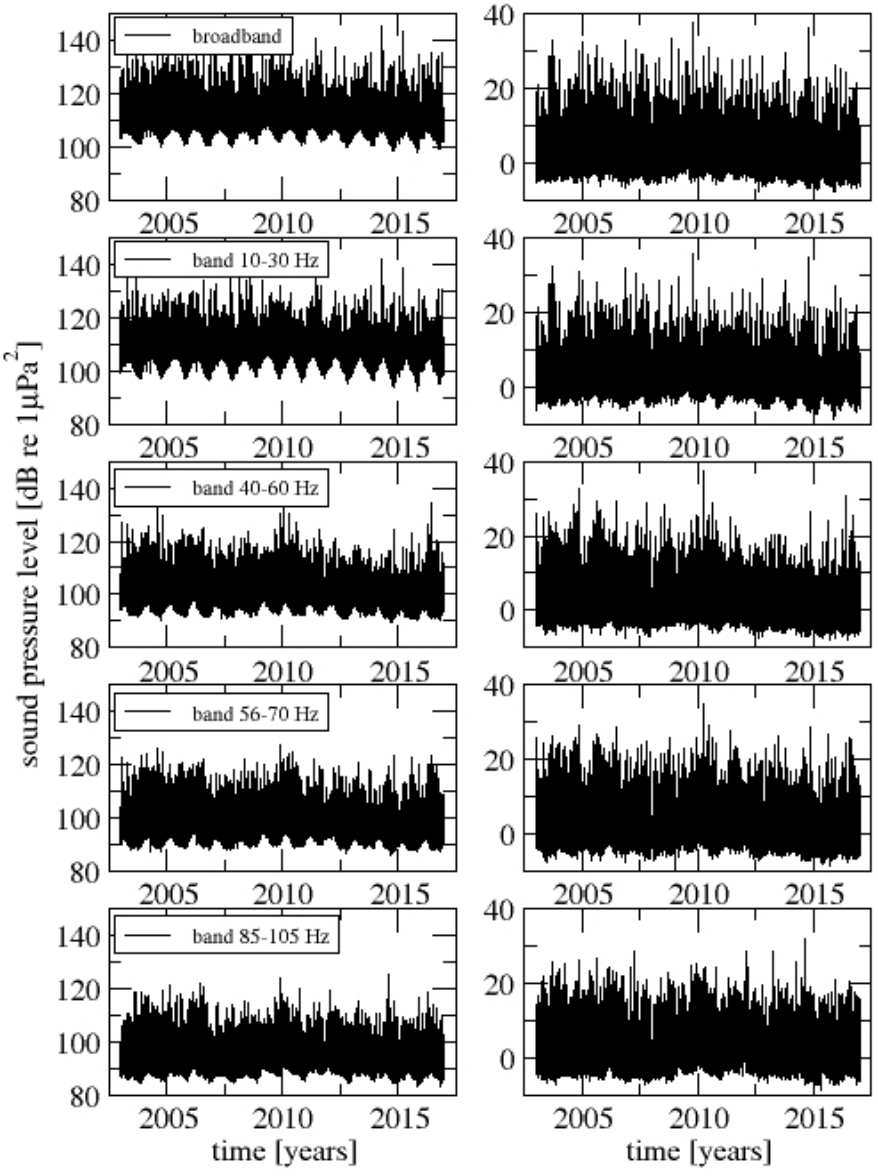

Fig. 1. Initial (left column) and processed (right column) sounds pressure level data in five frequency bands. Processing included interpolation and deseasonalisation. Note that seasonal variability is less pronounced in the higher frequencies of the initial data. At the same time, the records of higher frequencies have declining trend visible by eye.

Nonlin. Processes Geophys. Discuss., https://doi.org/10.5194/npg-2017-48
Manuscript under review for journal Nonlin. Processes Geophys.
Discussion started: 26 September 2017

4 Results and discussion

We analyse the global trends of these five datasets, assuming the simplest linear model in a least-square regression. To estimate the uncertainty in the trends, we apply the "jackknife" technique (see (Efron 1982) and (Wu 1986)). We use the "delete-d" variation of the method, with random subsampling and numerical implementation reducing the number of required samples, which allows to estimate variance of the trend as

$$v = \frac{r}{dm}\sum_{t=1}^{m}\left(T_{r,s_t} - \frac{1}{m}\sum_{k=1}^{m}T_{r,s_k}\right)^2, \tag{10}$$

where d is the number of the excluded datapoints in each sample ("delete-d"), $r = n - d$, T are statistics of the trend estimator, see further details in (Shao and Tu 1995).

The resulting trends show a small annual decline in SPL for all five datasets, as shown in Figure 2.

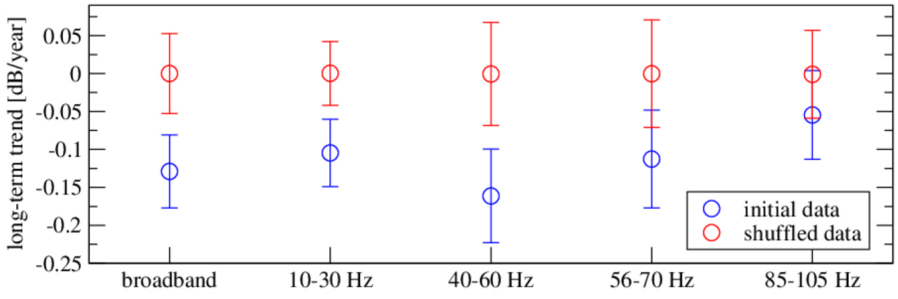

Fig. 2. Trend estimation in SPL bands (deseasonalised data) using "delete-d" jackknife sampling with 1000 subsets with d=10000 randomly deleted datapoints. Blue dots show the slope with corresponding jackknife uncertainties of the least-square linear regression, whereas red dots show the trend (the absence of it, with zero slopes of linear regression) for the shuffled data, i.e. the data with randomly allocated values of the time series.

The above trend analysis was applied to deseasonalised fluctuations (SPL broadband). It is interesting that the average annual cycle of the initial broadband data, too, has declining trend, which is illustrated in Figure 3.

The origin of the seasonality in the acoustic data from a hydrophone installed at depth is a subject of discussion, because the seasonal ocean temperature fluctuations at the surface would barely influence the sound propagation towards hydrophones. There are various possible mechanisms through which seasonal variability may manifest in the hydroacoustic data. For example, seasonal variations in shipping frequency, recreational vehicle use, iceberg breakup. Seasonally, there may be a slight warming/cooling in the top few tens of metres of water surface layer, but at the depth of the SOFAR (Sound Fixing and Ranging) channel temperature is stable on a seasonal timescale. Some seasonal

Nonlin. Processes Geophys. Discuss., https://doi.org/10.5194/npg-2017-48
Manuscript under review for journal Nonlin. Processes Geophys.
Discussion started: 26 September 2017

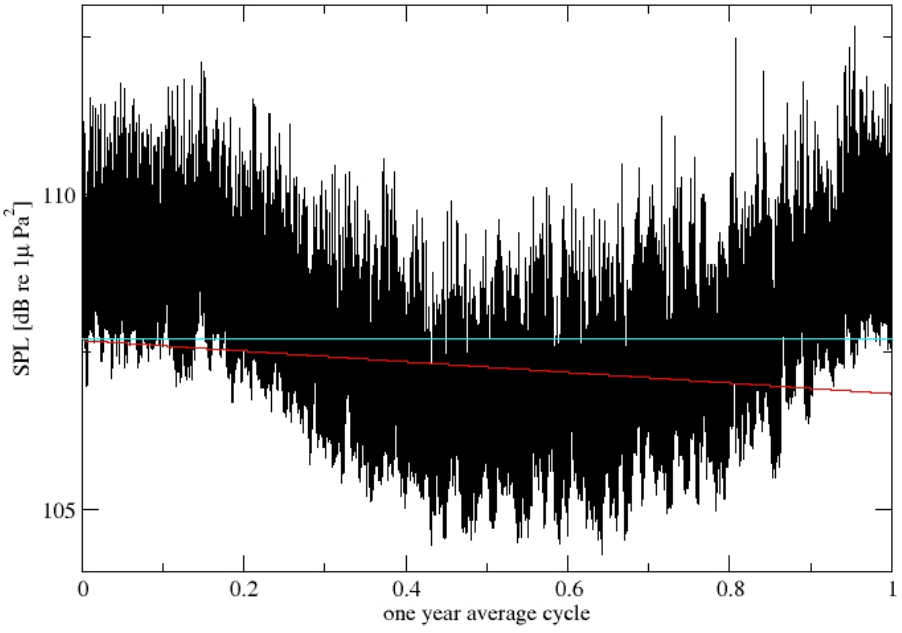

Fig. 3. Average annual cycle of the SPL broadband, its linear regression line (red) and horizontal line (cyan) for comparison.

effects in the sound record may be originating from iceberg formation as the edges of the Antarctic, as there are slightly faster ice crumbling in the southern-hemisphere summertime. Furthermore, seasonal variations in whale song are plausible, as well as in fauna migration due to seasonal fluctuations in food supply.

We next apply the pre-tipping analysis (early warning signals) to analyse lag-1 autocorrelations and variance of the broadband SPL record, with estimation of uncertainty. We vary the length of the sliding windows for calculating these indicators between 1/4 and 3/4 of the record length to obtain the averaged curves and standard uncertainties and display the indicator values at the end of each window, as shown in Figure 5. Similarly to CTBTO data, the effect of increasing autocorrelation and decreasing variance was earlier observed in bifurcating artificial data changing from white noise to random walk, in (Livina et al 2012). The acoustics dynamics may be undergoing a similar tipping. Note that this analysis of early warning signals is performed with large enough windows (starting from length of 3 years up to 9 years), which identify large-scale variability, with possible dynamics on the scale of decades ahead.

Further, we apply potential analysis to identify smaller-scale variability, varying the length of the sliding window from three days to one year. The resulting potential plot is shown in Figure 5.

El Niño/Southern Oscillation (ENSO) can be monitored using several indices. We show in Fig-

Nonlin. Processes Geophys. Discuss., https://doi.org/10.5194/npg-2017-48
Manuscript under review for journal Nonlin. Processes Geophys.
Discussion started: 26 September 2017

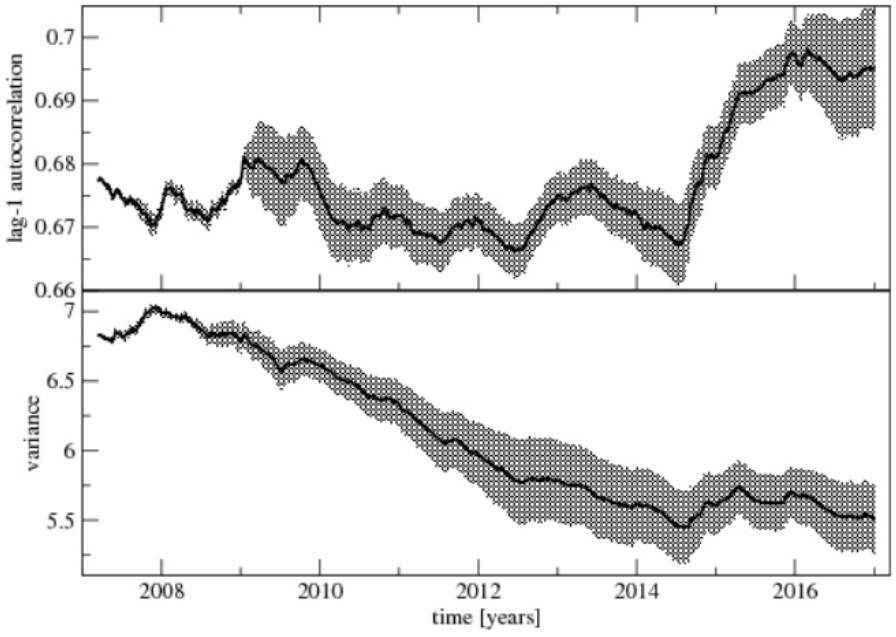

Fig. 4. Early-warning indicators of the broadband SPL dataset: lag-1 autocorrelation (upper panel) and variance (lower panel), calculated with variable window lengths, from 1/4 to 3/4 of the record length, and corresponding standard uncertainties, displayed at the end of each window. Both indicators demonstrate nonstationary behaviour (increasing autocorrelation and decreasing variance), which denotes long-term development of a possible tipping in future.

ure 5 two of them: Southern Oscillation Index (SOI) and Oceanic Niño Index (ONI). SOI is based on the sea level pressure differences between Tahiti and Darwin, Australia. ONI is based on the 3-month running mean of sea-surface temperature anomalies ERSST.v4 SST (Huang et al 2014) in the Niño 3.4 region (NOAA SOI index). Negative SOI (positive ONI) correspond to El Niño events, characterised by warm SST in the eastern and central tropical Pacific (Trenberth and Caron 2000).

To understand better what dynamical changes occur in the acoustic fluctuations, it is useful to plot the histograms of the corresponding subsets of data. Figure 6 demonstrates the difference between the 2-well-potential (first part of the year 2016) and the 3-well-potential (second part of the year 2016) subsets, which correspond to green and cyan areas in Figure 5.

The variability of the potential can be understood as appearance and disappearance of the SPL fluctuations, which are present in the 3-well-potential subsets and disappear in sub-periods of 2-well-potential dynamics. These periods of change seem to coincide with some of the recent El Niño events, in particular the strong oscillation in 2015-2016. Since in these short periods data become two-well-potential during El Niño, one can hypothesise that the El Niño event reduces acoustic

Nonlin. Processes Geophys. Discuss., https://doi.org/10.5194/npg-2017-48
Manuscript under review for journal Nonlin. Processes Geophys.
Discussion started: 26 September 2017

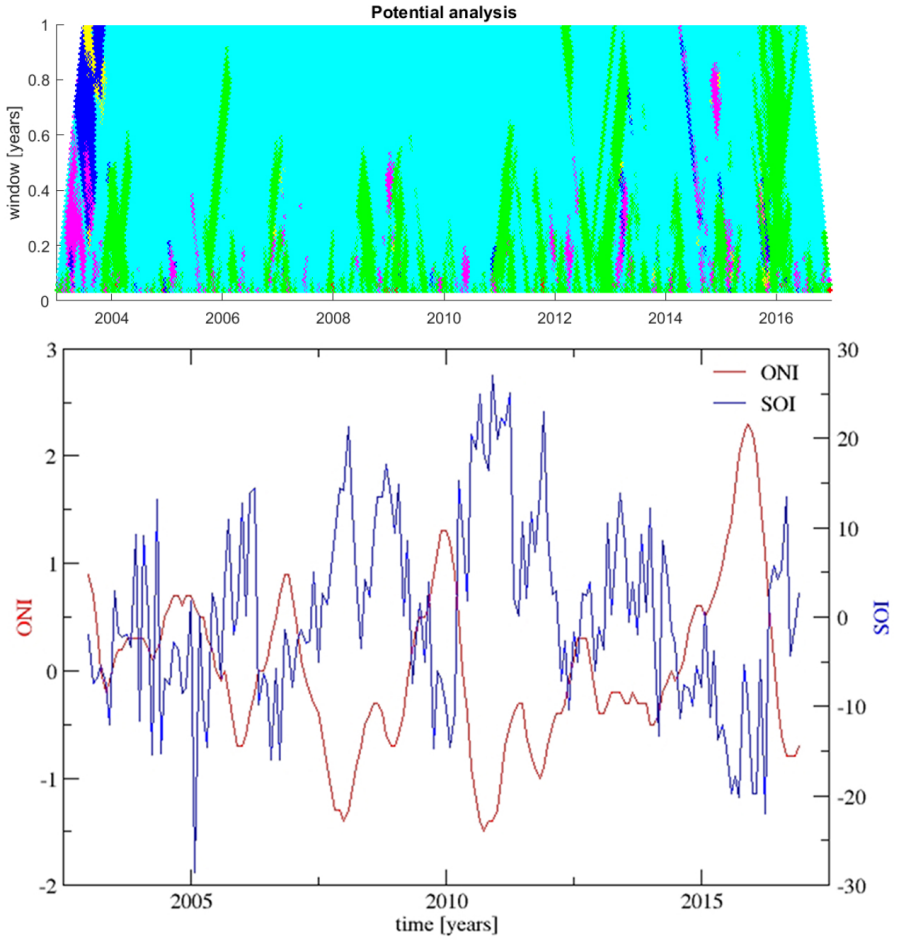

Fig. 5. Upper panel: potential analysis plot of the broadband SPL data, with varying window length (y-axis) from one day to one year. The colours denote the number of detected potential states: green two, cyan three. Specks of magenta denote very short periods of a higher number of states, which correspond to highly variable (possibly non-potential) subsets of data of small size. Lower panel: ENSO indices ONI and SOI, known to be anti-correlated, which indicate several ENSO events (El Niño and La Niña). These can also be seen in the potential analysis plot.

fluctuations events in the tails of the probability distribution (higher and lower values) and intensifies the events in the middle range of values.

It is known (Feng et al 2003) that the Leeuwin Current is influenced by El Niño, which causes lower temperature and slower current. This causes a number of climatic and environmental changes (including the impact of El Niño on sea level, current transport, and migration of marine animals),

Nonlin. Processes Geophys. Discuss., https://doi.org/10.5194/npg-2017-48
Manuscript under review for journal Nonlin. Processes Geophys.
Discussion started: 26 September 2017

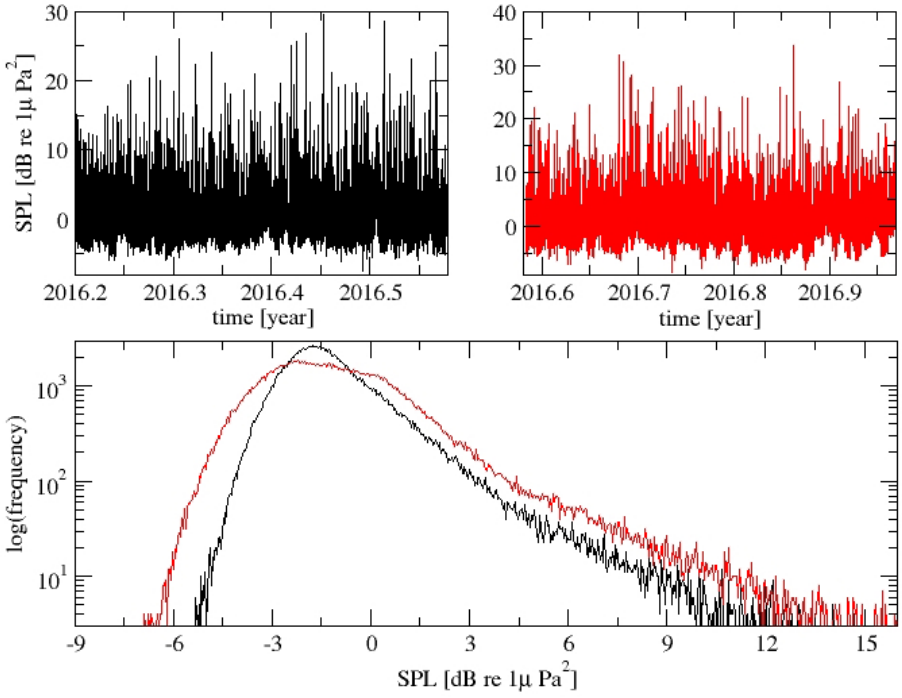

Fig. 6. The difference between 2-well-potential (first half of the year 2016, black curve) and 3-well-potential (second half of 2016, red curve) subsets of the broadband SPL record in the two upper panels. In the lower panel, the build-up of the new potential well can be seen in the red histogram, where the main mode becomes broader and starts building two new modes around SPL values -3 and 0 dB re 1 Pa^2 (deseasonalised SPL data).

and this may affect the acoustic signal. In particular, the local sea bottom slopes near Cape Leeuwin are very steep, with large underwater peaks (see Figure 4 in (Feng et al 2003)), which may be inducing reflection and scattering of the acoustic signal at greater depths, where the hydrophone is located.

Because the considered data is obtained from a hydrophone oriented in the west direction (towards the Indian ocean), one would expect very little influence on distant deep sources in predominantly west or south-westerly direction as their ray paths sample mostly the non-shallow ocean far removed from the coast and only passing through the Leeuwin Current at the last stage. But for surface-originating sounds from other directions there may well be an impact: where the sea bottom slopes through the SOFAR channel, particularly if it does so steeply, surface sounds and seismic waves can be reflected or refracted into the SOFAR channel. Note that on account of the lower speed of sound in water compared to rock, refraction is towards the normal for seismic waves coupling into water so such coupling is not efficient for a mostly horizontal sea bottom: the hydrophone array

Nonlin. Processes Geophys. Discuss., https://doi.org/10.5194/npg-2017-48
Manuscript under review for journal Nonlin. Processes Geophys.
Discussion started: 26 September 2017

will predominantly see seismic waves that impinge close-to-vertically from below (have a small slowness, high apparent velocity across the array) which are subsequently scattered by the wavy sea surface instead of propagating coherently onwards. Hence steep slopes couple better.

The detailed analysis of directional acoustic propagation is out of scope of the current paper and may be analysed later elsewhere.

Finally, we analyse the scaling properties of the deseasonalised fluctuations of the broadband SPL to identify the type of noise present in this dynamical system. When the noise is white, the Detrended Fluctuation Analysis (DFA) scaling exponent has value 0.5, whereas red noise has values of the exponent higher than 0.5 (Peng et al 1994), with nonstationary red noise having exponent higher than 1 (random walk has exponent 1.5). The scaling exponent is estimating by fitting the fluctuation curve $F(s) \sim s^{\alpha}$ in a log-log plot, as shown in Figure 7. When we apply the scaling analysis to the deseasonalised broadband SPL, in both short and long temporal range it has a high exponent (about 0.9), which means that the acoustic fluctuations are stationary red noise, and this is how they should be modelled to represent accurately the stochastic term in Eq. (1).

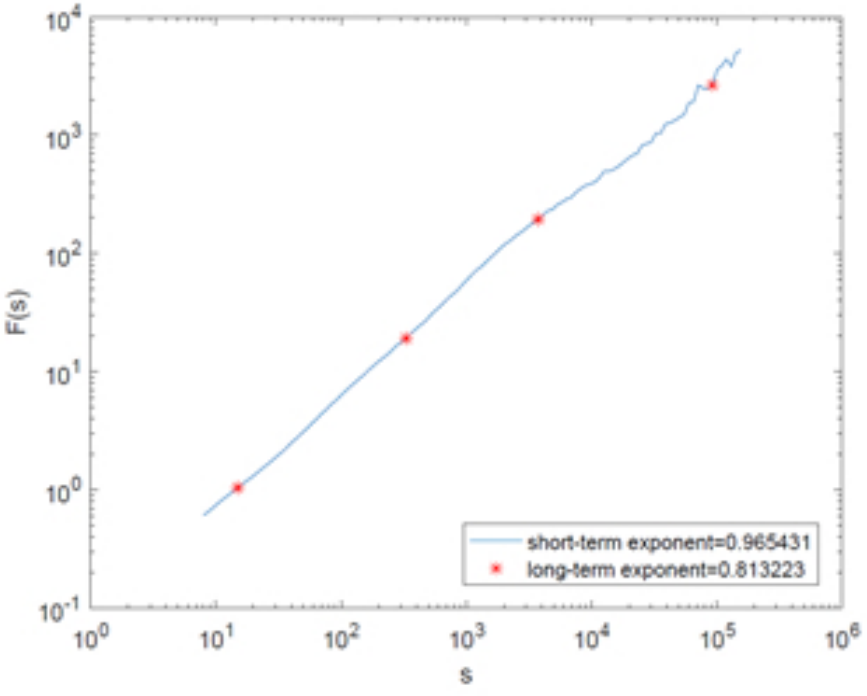

Fig. 7. Detrended Fluctuation Analysis scaling curve of the broadband SPL, with estimated scaling exponent values. The values are higher than 0.5, hence the noise is not white but red (with presence of correlations); the exponent is slightly smaller than 1, which means that the fluctuations are stationary (unlike a non-stationary random walk).

Nonlin. Processes Geophys. Discuss., https://doi.org/10.5194/npg-2017-48
Manuscript under review for journal Nonlin. Processes Geophys.
Discussion started: 26 September 2017

Nonlinear Processes in Geophysics
Discussions
Open Access
EGU

5 Model

Based on the above analysis, we can formulate a stochastic model for the acoustic oceanic noise. We adopt an additive model with the following terms:

$$z' = -U'(z,t) + T(t) + P(t) + \Phi, \tag{11}$$

where $U(t)$ is the system potential, $T(t)$ is a long-term linear trend, $P(t)$ is a seasonal trend, and Φ are red-noise fluctuations. In Equation 11, we use time as the main variable of the time series, assuming that only the shape of the potential U is defined by the state variable z as described above. The parameters of the model (the global trend slope, the amplitude of the seasonality, the coefficients of the potential, the scaling exponent of the fluctuations and the dynamics of its autocorrelation and variance) can be derived from the data and used for simulating artificial data for comparison. Such stochastically-modelled artificial data can be used for a long-term forecast of acoustic data and for testing various hypotheses of the hydroacoustic dynamical system. For simplicity, we illustrate this with a double-well potential term $U(t)$, and further parameters derived from the broadband SPL. We show five subsamples of the SPL broadband data in Figure 8, where observed and modelled time series are compared (left column), as well as their fluctuation curves (right column).

Conclusion

We have applied tipping point analysis and identified deterministic and stochastic components of the ocean acoustic data. We have discovered a possible signature of El Niño in the deep-ocean acoustic data, which is an interesting observation confirmed by both potential analysis and direct estimation of the probability density function of the broadband SPL. Given that the hydrophones are located at depth, and the number of factors influencing the hydroacoustic system in conjunction with the global climate system is large, the investigation of the transitional mechanisms between the surface multiannual phenomena and deep-water acoustic processes may be a subject of a separate paper. The current dynamics of the acoustic fluctuations, which demonstrate slow but steady changes in early warning indicators, gives indication of an upcoming tipping point in this hydroacoustic system, with possible appearance/disappearance of system states, which in this context denote higher/lower SPL fluctuations. Because Cape Leeuwin is a busy shipping junction in world trade, and as trading processes intensify (at the same time requiring more modern ships, with more efficient and less noisy engines), we hypothesise that frequency ranges of the oceanic acoustic noise will be affected unequally, due to multiple factors related to anthropogenic activities. Some frequency bands may decrease in level because of the technological changes: new developments in quieter engine technology, establishment of noise mitigation standards, and renewal of the fleets. In particular, there is global large-scale replacement of heavy-tonnage ships, where in some categories, like cargo, containers and bulk curriers ships of age above 25 years are no longer present, see the report of the European Maritime Safety

Nonlin. Processes Geophys. Discuss., https://doi.org/10.5194/npg-2017-48
Manuscript under review for journal Nonlin. Processes Geophys.
Discussion started: 26 September 2017

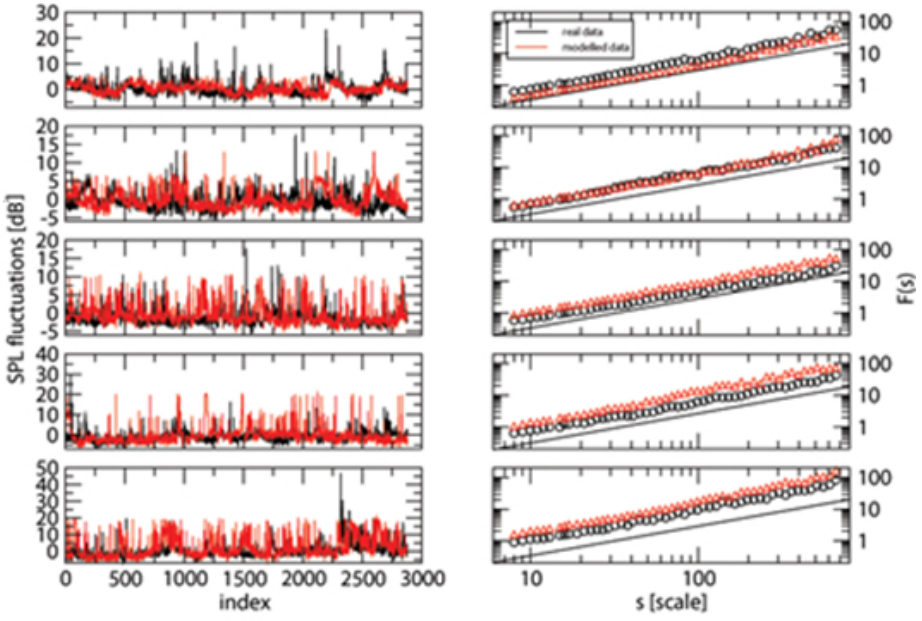

Fig. 8. Five samples of SPL data (real – black, modelled – red). Left column: samples of data; right column – DFA scaling curves. The thin line in the panels of the right column denotes the slope with scaling exponent 1, to which the curves are very close. The modelled data has the same probability density and scaling properties as the real data.

Agency (EMSA 2015).

Other potential causes of trends in ocean noise levels include changes in the frequency of other anthropogenic sources such as geophysical surveying, changes in the number and distributions of biological sources such as large cetaceans, changes in natural sources of sound such ice breaking and ice formation, and changes in the ocean environment which may affect the propagation of sound (for example, sea temperature). Whatever the potential causes, our analysis presents a possible approach for monitoring and modelling such processes in future.

Acknowledgement

The views expressed herein are not the opinion of the CTBTO. VL, PH, KS, LW, SR are funded by the National Measurement Office. The authors are grateful to the specialists of the virtual Data Exploitation Centre (vDEC) for providing the CTBTO data in their servers.

Nonlin. Processes Geophys. Discuss., https://doi.org/10.5194/npg-2017-48
Manuscript under review for journal Nonlin. Processes Geophys.
Discussion started: 26 September 2017

Nonlinear Processes in Geophysics
Discussions
Open Access
EGU

References

Cimatoribus, A, S Drijfhout, V Livina, and G van der Schrier, Dansgaard-Oeschger events: bifurcation points in the climate system, *Climate of the Past* **9** (2013): 323-333.

Commission, The Secretariat of the CTBTO Preparatory. Looking Back Over 15 Years. *Vienna: Provisional Technical Secretariat of the Preparatory Commission for the Comprehensive Nuclear-Test-Ban Treaty Organization*, 2013.

Dakos, V, et al. Methods for Detecting Early Warnings of Critical Transitions in Time Series Illustrated Using Simulated Ecological Data, *PLoS ONE* **7 (7)** (2012): e41010.

De Livera, A, R Hyndman, and R Snyder, Forecasting time series with complex seasonal patterns using exponential smoothing, *J. Am. Stat. Assoc.* **106** (2011): 1513-1527.

Efron, B. *The Jackknife, the Boostrap and other Resampling Plans.* Philadelphia: Society for Industrial and Applied Mathematics, 1982.

Feng, M, G Meyers, A Pearce, and S Wijffels, Annual and interannual variations of the Leeuwin Current at 32S, *Journal of Geophysical Research* **108 (C11)** (2003): 3355.

Held , H, and T Kleinen. Detection of climate system bifurcations by degenerate fingerprinting, *GRL* **31 (23)** (2004): L23207.

Huang, B, et al. Extended Reconstructed Sea Surface Temperature version 4 (ERSST.v4). *Journal of Climate* **28** (2014): 911-930.

ISO 18405:2017. Underwater Acoustics Terminology. International Organization for Standardization, Geneva, 2017.

Kantelhardt, J., S. Zschiegner, E. Koscielny-Bunde, A. Bunde, S. Havlin, and E. Stanley, Multifractal detrended fluctuation analysis of nonstationary time series, *Physica A* **316** (2002): 87-114.

Lenton, T, et al. Tipping elements in the Earths climate system, *Proceedings of the National Academy of Sciences USA* **105 (6)** (2008): 1786-1793.

Lenton, T, R Meyrscough, R Marsh, V Livina, A Price, and S Cox, Using GENIE to study a tipping point in the climate system, *Philosophical Transactions of the Royal Society A* **367** (2009): 871.

Lenton, T, V Livina, V Dakos, and M Scheffer, Climate bifurcation during the last deglaciation, *Climate of the Past* **8** (2012): 1127-1139.

Lenton, T, V Livina, V Dakos, E van Nes, and M Scheffer, Early warning of climate tipping points from critical slowing down: comparing methods to improve robustness, *Philosophical Transactions of the Royal Society A* **370** (2012): 1185-1204.

Livina, V, and T Lenton, A modified method for detecting incipient bifurcations in a dynamical system, *Geophys. Res. Lett.* **34** (2007): L03712.

Livina, V, E Barton, and A Forbes, Tipping point analysis of the NPL footbridge, *Journal of Civil Structural Health Monitoring* **4** (2014): 91-98.

Livina, V, F Kwasniok, and T Lenton, Potential analysis reveals changing number of climate states during the last 60 kyr, *Climate of the Past* **6** (2010): 77-82.

Livina, V, F Kwasniok, G Lohmann, J Kantelhardt, and T Lenton, Changing climate states and stability: from Pliocene to present, *Climate Dymamics* **37 (11-12)** (2011): 2437-2453.

Livina, V, G Lohmann, M Mudelsee, and T Lenton, Forecasting the underlying potential governing the time

series of a dynamical system, *Physica A* **392 (18)** (2013): 3891-3902.

Livina, V, P Ditlevsen, and T Lenton, An independent test of methods of detecting system states and bifurcations in time-series data, *Physica A* **391 (3)** (2012): 485-496.

Livina, V., and T. Lenton, A recent tipping point in the Arctic sea-ice cover: abrupt and persistent increase in the seasonal cycle since 2007, *Cryosphere* **7** (2013): 275-286.

NOAA SOI index. https://www.ncdc.noaa.gov/teleconnections/enso/indicators/soi/

Peng, C, S Buldyrev, S Havlin, M Simons, H Stanley, and A Goldberger, Mosaic organisation of DNA nucleotides, *Physical Review E* **49 (2)** (1994): 1685-1689.

Perry, M, P Niewczas, and V Livina, Tipping point analysis of cracking in reinforced concrete, *Smart Materials and Structures* **25** (2016): 015027.

Robinson S.P., Lepper P.A., Hazelwood R.A. Good Practice Guide for Underwater Noise Measurement. *NPL Good Practice Guide No. 133*, National Measurement Office, Marine Scotland, The Crown Estate, ISSN: 1368-6550, 2014.

Shao J. and D.Tu, it The Jackknife and Bootstrap, Springer Series in Statistics, 1995

The World Merchant Fleet in 2015. Annual Report, *EU: European Maritime Safety Agency*, 2015.

Trenberth, K., and J.Caron, The Southern Oscillation Revisited: Sea Level Pressures, Surface Temperatures, and Precipitation, *Journal of Climate* **13** (2000): 4358-4365.

Vaz Martins, T, V Livina, A Majtey, and R Toral, Resonance induced by repulsive interactions in a model of globally coupled bistable systems, *Phys. Rev. E* **81** (2010): 041103.

Wu, C. F. J., Jackknife, bootstrap and other resampling methods in regression analysis (with discussions), *Ann. Statist.* **14** (1986): 1261-1350.